Chapter 2

Two-Dimensional Correlation Analysis for Explosive Detection

2.1 INTRODUCTION

Improvised Explosive Devices (IEDs) are currently the number one killer of both troops and civilians in Iraq and Afghanistan.[1] Furthermore, world-wide IED events outside Iraq and Afghanistan number over 300 per month.[1] The ability to detect explosives prior to detonation would save lives; hence many laboratory techniques have been explored for explosive detection and classification (see reviews by Moore, 2004[2] or Steinfeld and Wormhoudt, 1998[3]). With the exception of the human eye and canine units, the most successful detection schemes are based on ion-mobility spectrometry, gas-chromatography/mass spectrometry, and fluorescence quenching of polymers. These all share the serious drawback of proximal sampling, which is extremely hazardous. An ideal system should quickly and accurately identify the presence of a variety of explosive traces in different environments with dynamic backgrounds at a safe standoff distance.

A possible solution to this complex problem is an optical-based scheme.[2, 3] Attempts have been made to utilize infrared (IR) spectroscopy,[4] photodissociation laser-induced fluorescence (PD-LIF),[5-7] laser-induced breakdown spectroscopy (LIBS),[8] and terahertz time domain spectroscopy (THz-TDS).[9] While well-suited for standoff detection, not all of these techniques meet the additional challenges of low vapor pressure of explosives and small sample size, as well as both optical and chemical interference – while requiring no sample preparation. However, even those techniques that are able to meet the challenges presented above suffer other serious drawbacks (for example, safety of implementation).[2-4, 10-12] This study focuses on a detection scheme based on long standoff Raman spectroscopy.[13-19]

Raman spectra provide direct information about molecular structure that can be used for identification. It is a non-invasive technique capable of analyzing both organic and inorganic compounds in any state (solid, liquid, gas), in most environments and without specific sample preparation requirements. The Raman Effect is the result of inelastic scattering of light from molecules that is shifted in frequency due to specific molecular vibrations. When an incident photon induces a dipole moment within a molecule, the result is a transfer of energy. If the molecule absorbs energy, the result is a photon scattered with less energy than the incident photon, or Stokes scattering. If, on the other hand, the molecule loses energy, the scattered photon will have greater energy and will be part of Anti-Stokes scattering. Stokes lines have greater intensity than Anti-Stokes lines at room temperature and are the focus of the current work.

The unique Raman signatures of many explosive materials are well known.[15, 20-29] The challenge is in obtaining these spectra from a distance of a few to hundreds of meters. Standoff systems often utilize a powerful, pulsed laser as the excitation source and a large optic to collect scattered photons that are sent to a dispersive spectrograph. Recent advances in optical-based standoff detection schemes have stemmed primarily from developments in the instrumentation of the detection system.[7, 11, 13, 14, 17-19, 30] However, long standoff detection of trace explosives presents a number of difficult challenges associated with rapid detection of a weak signal in a noisy and dynamic environment. Additional attempts have been made to enhance detection of explosives by exploiting their unique predisposition to decompose during heating.[21, 31-36] Another possible approach to increase the success of long standoff detection (based on any scheme) is through the analysis of spectra after collection, although this has received little attention.[12, 37, 38]

The system envisioned by Dr. Ravi Verma and Dr. Andrew Pipino at Tanner Research Inc. (Monrovia, CA) combines these three factors (hardware, material characteristics, and data analysis) to meet the challenges of long standoff Raman detection. Instrument design and assembly have been conducted by Dr. Andrew Pipino and includes a gated mechanism to minimize the amount of ambient light and luminescence that reaches the detector.[13, 30, 39] Once complete, the system would exploit the instability of explosives during incremental heating, which can be induced from a long standoff distance using a carbon dioxide (CO_2) laser. The enhancement in detection achieved by employing two-dimensional correlation spectroscopy is examined as part of this thesis. It was hypothesized that peaks characteristic of specific explosives would decrease as the explosive underwent thermal degradation while peaks corresponding to the decomposition products would increase. Furthermore, many of the potential interfering compounds in the operating environment have sufficient thermal stability that they would not be affected by the degree of heating used to induce thermal decomposition of energetic materials. The compounds that change due to heating would be selectively retained in the two-dimensional correlation spectra and the unchanged background would not contribute.

Two-dimensional (2D) correlation spectroscopy is a robust and versatile technique used to study molecular behavior as a function of a perturbation variable (e.g., temperature). Since its generalization by Noda,[40] the analysis has been applied to a variety of measurements across different fields.[41-49] Specifically, this analysis allows for separation of spectral features corresponding to explosives both from a noisy background and from any contaminants based on their rate of response to heating. Advantages of 2D correlation spectroscopy pertinent to detection include (1) simplification of complex

spectra by separation of overlapped peaks, (2) enhancement of spectral resolution and enhancement of signal to noise ratio (SNR) through the spreading of peaks over a second dimension, and (3) probing specific sequential order of spectral intensity changes.[50] In the current application, 2D correlation analysis should allow for rapid discrimination between unstable explosive traces and more stable contaminants, as the nature of the 2D approach is to eliminate static spectral features.

In this work, the concept of thermal decomposition in conjunction with 2D correlation spectroscopy for the detection of trace explosives was initially examined using a Raman microscope and a heating stage. Further investigations evaluated the two aspects of the analysis that can be used to further enhance detection: data pre-treatment and selection of the reference spectrum.

Data-pretreatments, such as smoothing, averaging, or normalization, can greatly enhance spectral features. In long standoff detection, a noisy background poses a significant challenge. This background can negatively affect SNR of synchronous spectra and sometimes produce artificial peaks in the asynchronous spectra.[51] Proper background subtraction is unrealistic due to the time-sensitive nature of the desired detection scheme, so alternatives must be considered. The effect of background scattering can be minimized through the use of first[52] and second[51] derivatives of the spectra. Alternatively, spectral normalization can also be utilized to enhance spectral features. In many cases, normalization schemes have little effect on qualitative results of 2D correlation analysis.[53, 54] However, in some studies, implementation of a normalization scheme has resulted in artificial peaks, especially in the asynchronous spectrum.[55-57] Given that the pre-treatment is dependent on and applied to each individual one dimensional (1D) spectrum, the following

correlation analysis may result in a significantly different SNR of the 2D spectra. Since the ultimate goal is to identify explosives while minimizing the probably of false negatives and false alarms, both derivates and a variety of normalization techniques were examined for greatest enhancement of explosive features in the 2D synchronous plot while minimizing the appearance of artificial peaks.

An additional variable in the 2D analysis that can be adjusted for better results is the reference spectrum selected for calculating the dynamic spectra. The selection of this reference spectrum is rather arbitrary;[50, 58] a simple option is to use an individual spectrum from the dataset.[47, 50, 58] Most commonly, the time-averaged (i.e., perturbation-averaged) spectrum is used, resulting in mean-centered dynamic spectra being analyzed.[40, 44, 59, 60] Each of these options was tested for the current application to determine which provided the best enhancement of explosive spectral features in the 2D synchronous plot, similar to the normalization schemes.

While noise is considered the greatest challenge of standoff detection, the ability to identify explosives in the presence of contaminants is not trivial. Therefore, additional studies were conducted to test the detection scheme in the presence of common interfering compounds. Finally, identification of trace explosive based on fine-tuned 2D correlation spectroscopy was demonstrated using the long standoff system at Tanner Research.

2.2   EXPERIMENTAL METHODS

2.2.1 Materials

For Raman Microspectroscopy experiments, cyclotrimethylenetrinitramine (RDX), pentaerythritol tetranitrate (PETN), 1,3,5,7-tetranitro-1,3,5,7-tetrazocane (HMX),

and trinitrotoluene (TNT) were purchased from Cerilliant at concentrations of 1000 μg/mL in acetonitrile (Figure 2.1). Neat residues of explosives were created by placing several drops of each solution onto glass slides and allowing the acetonitrile to evaporate under ambient conditions. For contamination studies, explosive solution was placed on glass slides in the presence of sand, saliva, urine, diesel soot and ester-terminated telechelic polybutadiene (PB; obtained from Materia) and allowed to dry.
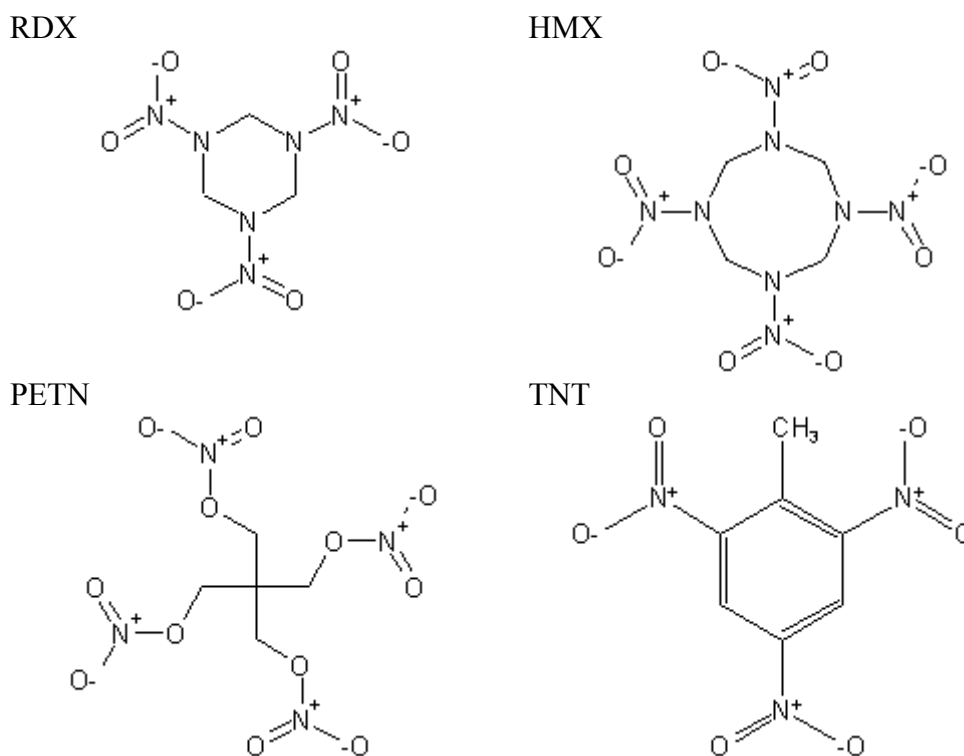
Figure 2.1 Molecular structure of the four military grade explosives examined.

For long standoff Raman experiments, 8 wt % RDX in a dry silica matrix (the most common constituent of sand) was purchased as a Non-Explosive Security Training and Testing (NESTT) product from XM division of Van Aken International. Approximately 10 grams of material as received was placed in a Petri dish at an approximate angle of 45° to the excitation beam.

2.2.2 Raman Microspectroscopy

Raman Microspectroscopy studies were conducted using a Renishaw MicroRaman Spectrometer in Professor George Rossman's laboratory in Caltech's Geological and Planetary Sciences Division with a continuous excitation wavelength of 514 nm and a grating size of 1800 lines/mm. The maximum power output from the excitation laser was 25 mW resulting in approximately 5 mW at the sample with a spot size of 30 μm. To simulate a thermal perturbation, a Linkam hot stage was used to heat samples at 10 °C/min while static spectra in the range of interest for each compound were acquired with acquisition times of 1.5 s. Maximum temperatures, which ranged from 150 to 200 °C were selected to achieve full conversion (i.e., disappearance of Raman signatures) of the explosive residues in order to obtain maximum features in the 2D correlation spectra, which measure the degree of change in a system. At the end of the heating ramp, 200 to 450 spectra were available for analysis.

2.2.2.1 Contamination Studies

Contamination studies proved difficult due to the small spot size of the Raman microscope excitation laser. Given the intrinsic heterogeneities in the sample and the 30 μm irradiated spot size, it was unfeasible to probe a representative average in the beam. As an alternative, detection of explosives in the presence of contaminants was evaluated by examining both multiple points on the same sample and multiple individual samples.

In the first scheme ('multi-point' experiment), a sample containing RDX, diesel soot, sand, and polybutadiene deposited from toluene solution was placed on a glass slide in a Linkam hot stage. Five points on the sample were selected based on visual inspection

through the microscope in an effort to obtain spectra of each material on the slide. A total of eight spectra were collected for each point as a function of temperature from room temperature up to 200 °C at discrete intervals of 25 °C. Temperature changes were conducted at 30 °C/min. One of the five points was excluded from the analysis due to large fluorescence, likely due to contamination at that point on the slide. The remaining four spectra were summed for each temperature to obtain a total spectrum representative of the whole sample at a particular temperature.

In the second scheme ('multi-sample' experiment), temperature-dependent spectra for individual materials collected during different experiments were summed and analyzed. Specifically, spectra for PETN, diesel soot, and bulk PB were collected during temperature ramps as described in Section 2.2.2. This procedure neglects any interaction that could occur between materials upon heating. However, this consequence does not appear to affect identification of explosive residue, which can be based on the disappearance of the energetic compound.

2.2.3 Long Standoff Raman Spectroscopy

Long standoff experiments were conducted by Dr. Andrew Pipino at Tanner Research. in Monrovia, California. The system, built by Dr. Pipino, utilized a frequency-doubled Nd:Yag laser (532 nm, 10 Hz) for sample excitation. A projection telescope was used to focus the excitation beam to a 2–3 mm spot on the sample approximately 9 m away. Excitation source power was approximately 0.1 watts at the sample. Data was collected using a Spectra Pro 2300i spectrometer (Princeton Instruments) set to a 50 ns gate delayed 107 ns from the trigger of the pulsed excitation source. This combination of gate

width and delay was experimentally optimized to maximize the scattering signal and exclude fluorescence based on the disparity in lifetimes between Raman scattering (10^{-13}–10^{-11} s) and fluorescence (10^{-9}–10^{-7} s).[13, 39, 61] Noise was further decreased through multi-spectra averaging: an average of 10 spectra each obtained by an additional 10-pulse detector average (1 spectrum every 10 s) was compared with single-pulse data and no averaging (1 spectrum every 0.1 s). Thermal modulation was accomplished with a carbon dioxide (CO_2, 10.6 μm) laser whose output was absorbed by the sand substrate. The laser was controlled by a transistor-transistor-logic (TTL) oscillator with a 50% duty cycle and a frequency of 0.1 Hz. CO_2 laser power was approximately 2 watts at the sample.

2.2.4 Computation

Two-dimensional (2D) correlation spectra were calculated using Noda's generalized method[40, 62] from a discrete set of spectra measured at m equally spaced points during a thermal perturbation:

$$y_i(v) = y(v, T_i) \qquad i = 1,2,3,\ldots,m. \tag{2.1}$$

A variety of data pre-treatments and normalizations (Table 2.1) were tested using a dataset that was affected by noise and light fluorescence (a set of PETN spectra), two of the challenges faced in the operational environment. Derivatives can be applied to highlight rapid changes in the system and allow for the elimination of a dynamic baseline offset.[51, 52] Mean normalization has the effect of assigning an equal distribution of variances to the data, resulting in spectra with equal areas.[59, 63] Modified mean normalization (MMN) accounts for differences in peak area and half width by approximating bands as Lorentzian peaks in order to de-convolute overlapping features.[64] Principal component

analysis (PCA) is a data-reduction technique that can be used to obtain a vector that

accounts for the greatest variation in the dataset containing all spectral points called the

first principal component, PC_1. This first principal component is an m-dimensional col-

umn vector $(PC_1=[pc_{11}, pc_{12}, ..., pc_{1m}]^T)$ with elements composed of linear combinations

of the original spectra: $pc_{1i} = a_{11}y_{i1} + a_{12}y_{i2} + ... + a_{1n}y_{in}$, where y_{ij} is the intensity at the jth

spectral variable in the ith spectrum containing n total points and the loadings, a, represent

the weights of each original spectral intensity in the calculation of the first principal com-

ponent.[65] All of these approaches normalize each spectrum by a constant that represents

the overall intensity in that spectrum. The simplest means of achieving this is through

Table 2.1 Summary of pre-treatments and normalizations tested on a noisy PETN dataset for best 1D and 2D synchronous performance parameter.

pre-treatment/normalization	$y_i(\nu)$
1st derivative with respect to Raman shift	$\dfrac{\partial y_i}{\partial \nu}$
1st derivative with respect to the perturbation variable[52]	$\dfrac{\partial y_i}{\partial T_i}$
2nd derivative with respect to Raman shift[51]	$\dfrac{\partial^2 y_i}{\partial \nu^2}$
2nd derivative with respect to the perturbation variable[51]	$\dfrac{\partial^2 y_i}{\partial T_i^2}$
Mean normalization [59, 63]	$\dfrac{y_i}{y_{i,mean}}$, where $y_{i,mean} = \dfrac{1}{(\nu_{max} - \nu_{min})}\int_{\nu_{min}}^{\nu_{max}} y_i(\nu)d\nu$
Modified mean normalization (MMN)[64]	$\dfrac{y_i}{C_i}$, where $C_i = \dfrac{y_{i,mean}^2}{y_{i,max}}$
Principal component normalization[65]	$\dfrac{y_i}{pc_{1i}}$, where pc_{1i} is the ith loading of the first principal component
Peak value normalization[66]	$\dfrac{y_i}{y_i(\nu = 1290)}$, where 1290 cm^{-1} is the position of the peak of interest for PETN

normalization by a specific peak value of interest.[66] The effectiveness of each treatment was evaluated based on the performance parameter (eq 2.2) of the 1D dynamic and 2D synchronous spectra, as well as a qualitative assessment.

To determine the effectiveness of signal detection, a performance parameter, P, is defined as the ratio of the variance of the signal to the variance of the background:

$$P = \frac{\sigma^2_{signal}}{\sigma^2_{bkgr}}.$$

$$(2.2)$$

For each material, well-defined 1D Raman spectra were used to select areas of the background that did not contain any Raman lines. The signal variance was defined for the primary Raman peak at 877 cm^{-1} for RDX, 844 cm^{-1} for HMX, and 1290 cm^{-1} for PETN (see Section 2.3.1.1). The performance parameter was calculated and averaged for 1D dynamic spectra following pretreatment. Comparisons were made with P values calculated for the corresponding 2D synchronous correlation spectra using the same baseline and signal ranges in two dimensions along the diagonal. The performance parameter is based on the definition of signal to noise ratio (SNR) commonly used in digital signal processing: variance of signal to variance of noise.[67, 68]

The discrete dynamic spectra, $\tilde{y}$, were calculated from the normalized data with respect to a reference spectrum, y_{ref}:

$$\tilde{y}_i(v) = y_i(v) - y_{ref}(v) \qquad i = 1,2,3,...,m.$$

$$(2.3)$$

Three options for y_{ref} were examined: (1) 1st spectrum of the set ($y_{ref}(v) = y_1(v)$), (2) last spectrum of the set ($y_{ref}(v) = y_m(v)$), and (3) time-averaged (or, in this case, temperature-averaged) spectrum:

$$\overline{y}(\nu) = \frac{1}{m} \sum_{i=1}^{m} y(\nu, T_i).$$
(2.4)

The reference spectrum yielding the highest performance parameter for the 2D synchronous spectrum (eq 2.2) was used for the remainder of the analysis.

The synchronous 2D correlation intensity, demonstrating simultaneous or coincidental changes in intensity, is given by

$$\Phi(\nu_1, \nu_2) = \frac{1}{m-1} \sum_{i=1}^{m} \widetilde{y}_i(\nu_1) \cdot \widetilde{y}_i(\nu_2).$$
(2.5)

The asynchronous 2D correlation spectra, showing decoupled changes in intensity, is given by

$$\Psi(\nu_1, \nu_2) = \frac{1}{m-1} \sum_{i=1}^{m} \widetilde{y}_i(\nu_1) \cdot \widetilde{z}_i(\nu_2),$$
(2.6)

where $\widetilde{z}_i(\nu_2)$ is the discrete orthogonal spectra resulting from a linear transformation,

$$\widetilde{z}_i(\nu_2) = \sum_{j=1}^{m} N_{ij} \cdot \widetilde{y}_j(\nu_2),$$
(2.7)

and N_{ij} is the Hilbert-Noda transformation matrix,

$$N_{ij} = \begin{cases} 0 & \text{if } i = j \\ \dfrac{1}{\pi(j-i)} & \text{otherwise} \end{cases}.$$
(2.8)

All 2D correlation computation and plot generation was conducted using MATLAB R2008a.

2.3 RESULTS

2.3.1 Raman Microspectroscopy of Pure Compounds

2.3.1.1 One-Dimensional Raman Spectra

The Stokes Raman spectra of the investigated compounds have been described previously.[19, 21, 23, 69] Of particular interest in long standoff detection is the range of 150 to 3500 cm^{-1} containing a number of unique molecular signatures that can be used to identify RDX, HMX, and PETN (Figure 2.2). For RDX, the cluster of peaks in the range of 1200 to 1500 cm^{-1} is due to symmetric NO_2 and N-N stretches. The peaks in the range of 500 cm^{-1} are the result of ring torsion. The primary peak at 877 cm^{-1} and the few surrounding it are caused by ring stretch.[21] HMX, being a nitramine explosive like RDX, has many similar features. There are signatures of symmetric NO_2 and N-N stretches in the region of 1200 to 1500 cm^{-1}.[19] Although not as prominent, its primary peak at 844 cm^{-1} is due to ring stretching.[23] HMX has an additional broader peak in the range of 1100 to 1200 cm^{-1} also attributed to ring stretching.[19] The peak at approximately 1550 cm^{-1} is due to anti-symmetric stretching of NO_2 groups.[69] The spectral features of PETN include a relatively broad peak at approximately 1650 cm^{-1} due to anti-symmetric NO_2 stretching and a sharp peak at 860 cm^{-1} attributed to the O-N stretching mode. The strong peak at 1290 cm^{-1} is due to symmetric stretching of the nitro groups.[23] The strong peaks common to all three explosives at 3000 cm^{-1} are due to aliphatic CH stretching and overlap with abundant species (organic matter) in the operating environment. Although it is possible to distinguish between different types of explosives (e.g., nitramines like RDX versus nitroaromatics like TNT) through careful evaluation of these bands (relative intensity and band width),[23] the required analysis is too time-consuming for the current application, es-

pecially if mixtures of explosives are used. Unfortunately, due to large fluorescence, distinguishable TNT peaks were not observed.
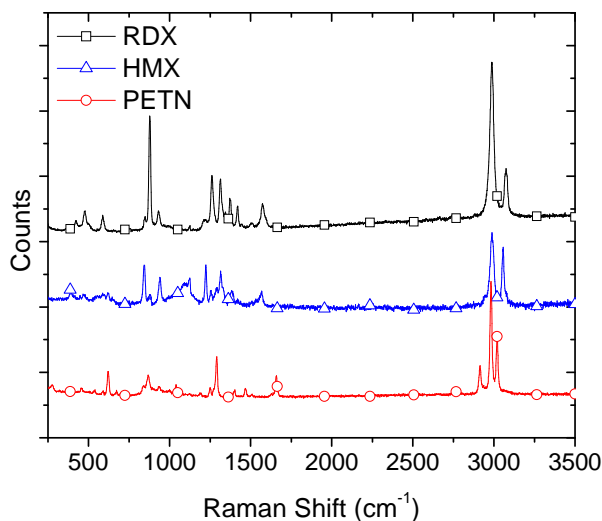
Figure 2.2 Raman spectra of explosive residues.

For preliminary studies, cropped ranges were selected for each material to achieve rapid detection. These 'areas of interest' were selected to include the most intense peaks (excluding the region around 3000 cm^{-1} as mentioned above) for each material as these would exhibit the greatest change upon full conversion of the explosive. From Figure 2.2, these peaks are at 877 cm^{-1} for RDX, 844 cm^{-1} for HMX, and 1290 cm^{-1} for PETN.

2.3.1.2 Clean Two-Dimensional Correlation Spectra

Two dimensional correlation analysis was applied to "clean" (high SNR, flat baseline) sets of RDX and HMX spectra in a narrow range. During the heating ramps, no new Raman peaks appeared in the 1D spectra that could correspond to decomposition products. Rather, all features of the explosive compound decreased and eventually disap-

peared. Corresponding 2D correlation spectra show distinct peaks for both materials that can be used to identify the explosives. In the synchronous spectrum of RDX (Figure 2.3a, left), only one strong autopeak is observed on the diagonal at 878 cm^{-1}. However, positive cross peaks at 848 and 932 cm^{-1} indicate that there are weaker autopeaks at those Raman shifts which are not much higher than the baseline. All cross peaks are positive, indicating that upon heating, all of the RDX peaks change in the same direction—that is, they decrease. The asynchronous plot shows a tight four-leaf pattern centered at the primary RDX peak (Figure 2.3a, right). The corresponding pairs of peaks are located adjacent to the main peak at (1) 885 and 878 cm^{-1} and at (2) 870 and 878 cm^{-1} and do not correspond to multiple peaks in the 1D spectrum (inset in Figure 2.3a, right). This unexpected pattern can be understood in terms of the crystal structure of the materials as discussed later. The light streaks in the asynchronous plot are due to noise in the background which contributes random fluctuations that are then magnified by the primary RDX peak.[51]

The synchronous spectrum for HMX is slightly more complex containing more auto- and cross peaks (Figure 2.3b, left). The strongest peaks are those forming a correlation square defined by the autopeaks at 844 and 940 cm^{-1}. Similar to RDX, all of the peaks appearing in the synchronous spectrum are positive. The asynchronous spectrum again shows streaking as a result of background noise (Figure 2.3b, right). The increased intensity of streaks at larger Raman shift values indicates that there are larger background fluctuations at those spectral values. Additionally, similar to RDX, concentrated pairs of cross peaks corresponding to the vertices of the correlation square are observed due to the crystalline nature of HMX: (1) 844 and 851 cm^{-1} and (2) 940 and 945 cm^{-1}.
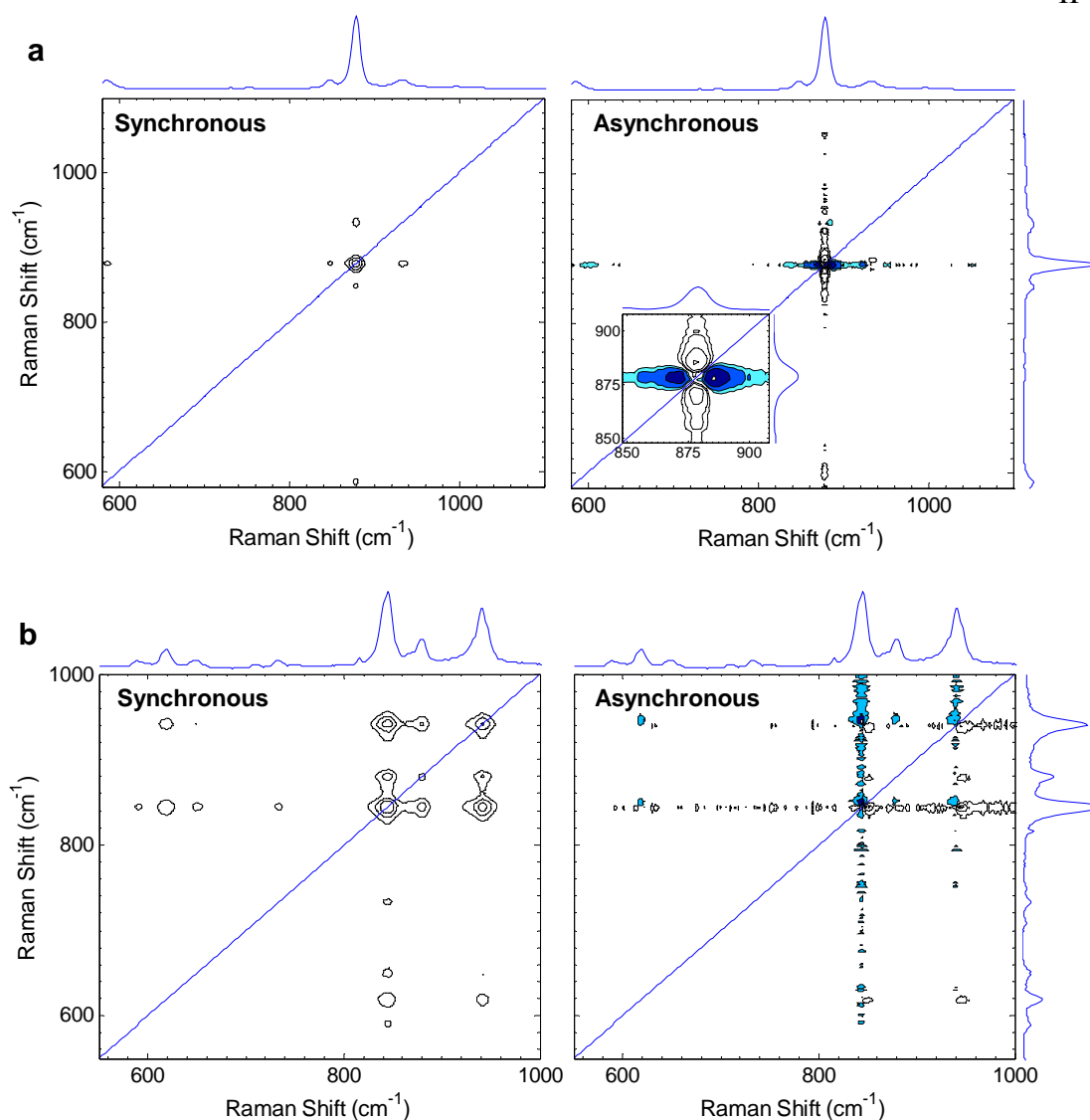
Figure 2.3 2D synchronous (left) and asynchronous (right) correlation spectra during heating ramps for **a)** RDX and **b)** HMX. Positive and negative contours are shown as open and filled, respectively. Averaged 1D spectra are shown on the sides.

Application of the 2D correlation analysis results in much greater values for the performance parameter, *P* (Table 2.2). In the cases of these well-defined RDX and HMX spectra, improvements in *P* are multiple orders of magnitude. Increased values of *P* lead to improved discrimination between peak values of interest and baseline scattering as can be seen in histograms of intensity values. As demonstrated in an example of HMX in

Figure 2.4, the 2D nature of the analysis significantly increases peak values (as a

result of peak-peak correlation) and minimizes baseline (as a result of weak or absent cor-

relation).

Table 2.2 Performance parameters and their ratios for RDX[a], HMX[a], and PETN[b].

Sample	P_{2D}[c]	P_{1D}[d]	P_{2D} / P_{1D}
RDX	6.7×10^6	2.9×10^2	2.4×10^4
HMX	1.2×10^5	3.2×10^1	3.7×10^3
PETN, no treatment	3.1×10^2	3.4×10^1	9.0×10^0
PETN, floored	2.7×10^4	3.4×10^1	8.1×10^2
PETN, MMN	1.4×10^5	2.5×10^2	5.7×10^2

[a]Figure 2.3
[b]Figure 2.6
[c]P_{2D}: performance parameter for synchronous 2D spectrum
[d]P_{1D}: average performance parameter for 1D dynamic spectra
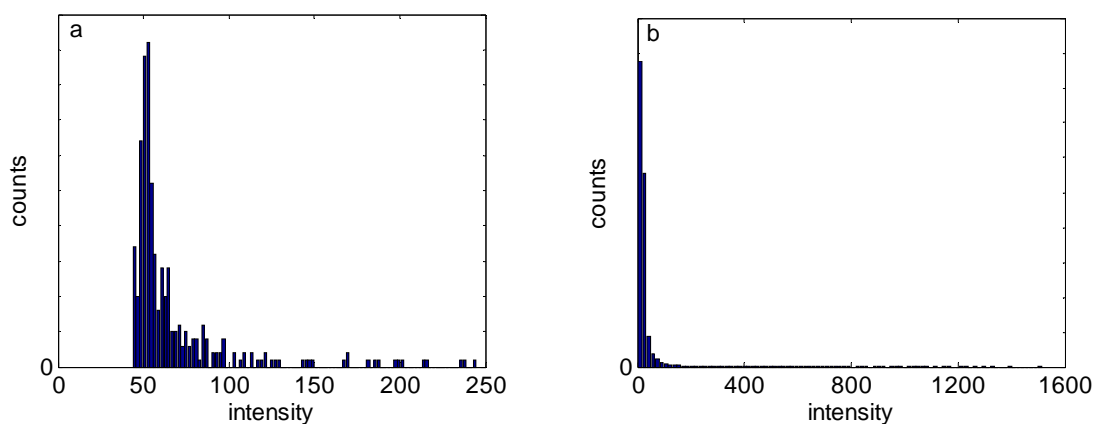
Figure 2.4 Histogram plots of intensity values for **a)** 1D and **b)** 2D synchronous spectra of HMX corresponding to Figure 2.3b.

2.3.1.3 Effect of Background in Two-Dimensional Correlation Spectra
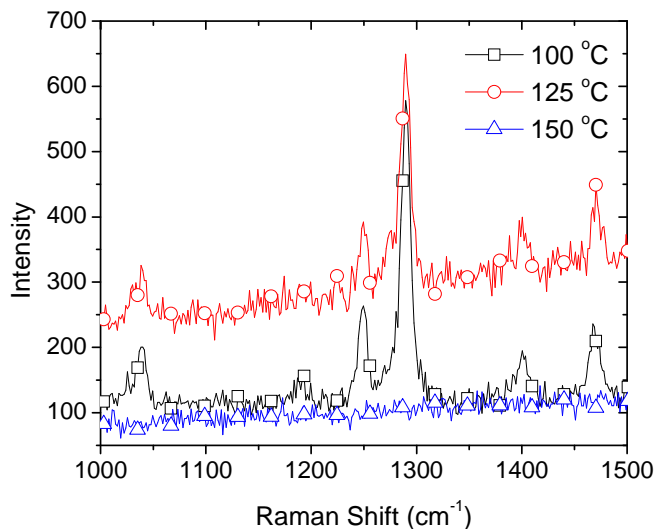
Figure 2.5 Raman spectra of PETN collected at select temperatures during heating ramp.

In contrast to s pectra containing strong peaks and flat baselines (RDX and HMX above), challenges arose when individual spectra, $y_i(v)$, exhibited a varying fluorescent background. The development of mild fluorescence was evident in a set of PETN spectra (Figure 2.5), where the background remained stationary at temperatures below 100 °C, grew at higher temperatures as the magnitude of PETN peaks began to decrease, and dropped again near the highest temperatures once PETN peaks disappeared. These observations are consistent with previous studies on time-dependent luminescence following decomposition of PETN.[70]

Fluorescence is characterized by larger intensity at larger Raman shift, which is manifested in the 2D synchronous spectrum as excess background noise and heavy streaks corresponding to the strong PETN features (Figure 2.6a). Since the growth of fluorescence coincided with a change in PETN features but did not follow the same

monotonic trend, the asynchronous spectrum also exhibits heavy streaking. Although the primary PETN peak at 1290 cm^{-1} is evident in both the synchronous and asynchronous plots, the observed streaks are undesirable since they may mask the presence of weaker peaks of significance. Additionally, from Table 2.1, it is evident that the floating background negatively affects the synchronous performance parameter.
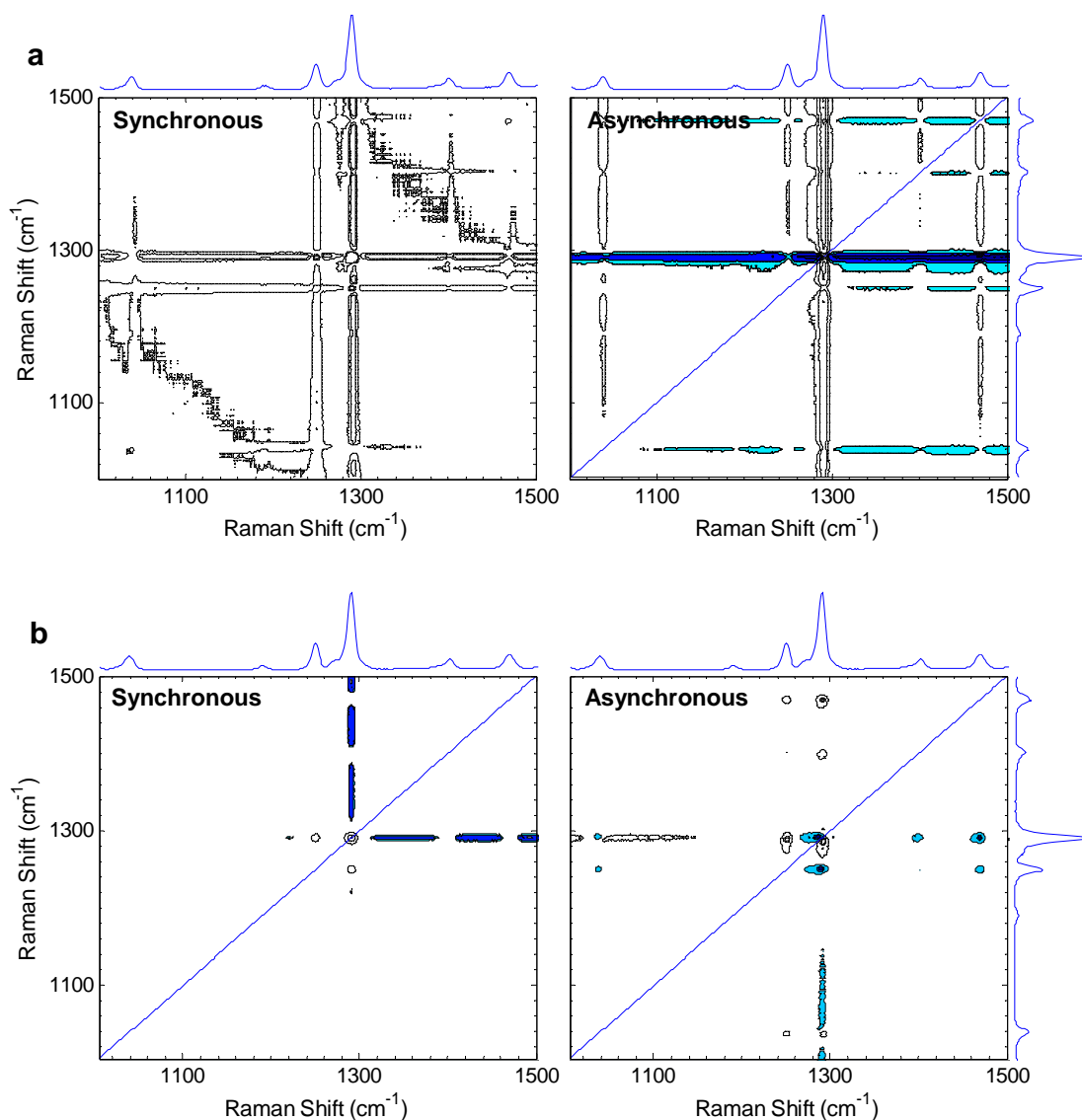
Figure 2.6 2D synchronous (left) and asynchronous (right) correlation spectra during heating ramps of PETN: **a)** no data pre-treatment **b)** flooring followed by modified mean normalization applied to each 1D dynamic spectrum. Positive and negative contours are shown as open and filled, respectively. Averaged 1D spectra are shown on the sides.

The initial approach employed to handle the adverse effects of this non-static background was to subtract the minimum value from each spectrum prior to calculating the dynamic spectra.[51] This 'flooring' treatment, compensates for the dynamic baseline offset and results in an improvement of two orders of magnitude in P_{2D} in the current case. However, the tilt in the background remains, as do the streaks in the 2D spectra at higher Raman shift.

Modified mean normalization[64] of each dynamic spectrum results in cleaner corresponding 2D spectra (Figure 2.6b). In the synchronous spectrum, the primary PETN peak is clearly identified, in addition to a number of cross peaks corresponding to other PETN features. The appearance of negative, elongated cross peaks associated with the primary peak (located in line with 1290 cm^{-1} and extending to larger Raman shift values) are consistent with simultaneous increase of fluorescence and decrease of the Raman peak at 1290 cm^{-1}. In the asynchronous plot, the streaks are diminished revealing a pair of elongated cross peaks close to the diagonal corresponding to the primary PETN peak at 1290 cm^{-1}. Furthermore, there are a number of cross peaks in the asynchronous spectrum corresponding to separate PETN features which suggests that the changes in these peaks are not fully synchronized. Care must be exercised in assigning these features: the observation could be an artifact of the normalization or the result of the crystalline nature of PETN and will be discussed later. Finally, mean normalization increases both the 1D and 2D performance parameter by an additional order of magnitude (Table 2.2).

2.3.1.4 Data Pretreatment

Encouraged by the increase in P as the result of normalization (above), a number of common data pretreatments (Table 2.1) were tested for efficacy in minimizing the effects of noise and background on the performance parameter of the synchronous 2D spectra. All data pretreatments examined affected both the 1D and 2D performance parameter. Although one would normally expect P_{1D} to remain unchanged after normalization by a constant, this is not the case when constants are spectrum-dependant and P is evaluated for dynamic spectra. When each spectrum is normalized by a unique constant defined by the values in that spectrum, the result is an average spectrum that is no longer linearly related to the average spectrum prior to normalization. Hence, the normalized dynamic spectra will have a different value of P.

The first four pretreatments are based on differentiation and have sometimes resulted in enhanced spectral features.[51, 52] While differentiation minimizes adverse effects of a tilted baseline, it also increases the effects of noise. In the present case, these pretreatments reduced P for both the 1D dynamic and 2D synchronous spectra of PETN (Figure 2.6a) and, hence, were excluded from further analysis.

Table 2.3 Performance parameters and their ratios for floored PETN spectra corresponding to Figure 2.6a treated with different normalizations (Table 2.1).

	Mean Normalized	Modified Mean (MMN)	Principal Component, PC_1	Peak Normalized, $y(v=1290\ \mathrm{cm}^{-1})$
$P_{2D}{}^{a}$	6.2×10^4	1.4×10^5	5.0×10^4	1.7×10^1
$P_{1D}{}^{b}$	3.8×10^1	2.5×10^2	1.9×10^2	5.4×10^0
P_{2D} / P_{1D}	1.7×10^3	5.7×10^2	2.6×10^2	3.2×10^0

$^{a}P_{2D}$: performance parameter for synchronous 2D spectrum
$^{b}P_{1D}$: average performance parameter for 1D dynamic spectra

Of the remaining four normalization schemes (outlined in Table 2.3), the least effective (lowest P) was normalizing the raw data, $y_i(v)$, by the intensity value of the primary PETN peak at 1290 cm^{-1}. This result is not surprising given the nature of PETN disappearance that is at the center of this detection scheme. Normalization by the peak value would be more effective if the peak exhibited only minor intensity changes. However, given that, at the end of the experiment, the intensity at 1290 cm^{-1} is comparable to the background, the background intensities of these spectra are assigned equal weight by the treatment subsequently resulting in very noisy correlation spectra. Of the normalization methods examined, modified mean normalization (MMN) yielded both the highest P_{1D} and P_{2D} by an order of magnitude. While it may seem desirable to apply modified mean normalization to all further analysis, care must be taken as sometimes artifacts appear in the resulting spectra.[57]

2.3.1.5 Reference Spectrum

The selection of a reference spectrum can be adjusted in the 2D correlation analysis to yield optimal results.[50, 58] Of the three possibilities examined (Section 2.2.4), the temperature-averaged spectrum (eq 2.4) gives the greatest value for performance parameter for the 2D synchronous spectra for all cases analyzed. Relative to using the first or last spectrum (i.e., $y_1(v)$ or $y_m(v)$) as a reference, which both contribute similar noise to that already present in each $y_i(v)$, subtracting the average spectrum from each $y_i(v)$ has the advantage of the reference contributing noise that is reduced by $m^{-0.5}$. Although it has been suggested that no reference spectrum can be useful when data are excessively noisy,[51] the use of a reference spectrum is necessary to achieve removal of stationary peaks from 2D

spectra. Hence, the temperature-averaged spectrum was used to calculate the dynamics spectra for all of the results presented.

2.3.2 Raman Microspectroscopy: Contamination Studies

A further challenge for the 2D correlation approach is to identify explosives in the presence of common contaminants. Additionally, it is of interest to understand how explosives behave in the presence of such contaminants under heating and the consequent effects on the 2D spectra. Although several studies have found that the presence of sand or soil does not affect Raman signatures of some military-grade explosives, to our knowledge, temperature effects were not examined in prior literature.[20, 22]

Contamination studies were performed using protocols suitable for the MicroRaman spectrometer used for this work. As noted in prior literature, luminescence can severely interfere with acquisition of Raman spectra.[13, 71] A highly fluorescent yet common contaminant in the operating environment is urine.[72] The spectrometer used for the present thermal oxidation experiments was not equipped with gating, and urine was observed to mask the signal from any other compounds present in the sample. Consequently, detection of explosives in the presence of urine could not be tested using the Renishaw MicroRaman spectrometer. In view of the small size of the irradiated area, which made it difficult to ensure multiple materials in a heterogeneous specimen were adequately sampled in the beam, two alternative methods were used in addition to traditional contamination studies: multi-point and multi-sample experiment. The following three case studies are presented to gauge the effectiveness of 2D correlation analysis for explosive detection in the presence of different contaminants.

2.3.2.1 Traditional: RDX and Saliva on Sand

A traditional contamination study, in which multiple specimens were in the beam and undergoing simultaneous thermal treatment, was successful for a sample containing trace RDX and saliva on sand, which is primarily composed of quartz. In the full range examined (Figure 2.7a), both the 1D and the 2D spectra were dwarfed by the quartz peak at 460 cm^{-1}. The presence of the quartz peak in the 2D spectra is surprising given that this stable substance is not expected to undergo chemical changes at the moderate temperatures employed (<200 °C). However, the crystal nature of quartz results in slight shifting and broadening of the Raman feature with increasing temperatures, which is apparent in the 2D spectra.[73, 74] Further evidence for this explanation is apparent in the asynchronous spectrum which displays a pair of cross peaks near the diagonal corresponding to the quartz Raman feature, which are known to be present in cases of minor peak shifting and broadening.[50, 51] The 2D synchronous plot (Figure 2.7a, left) also exhibits autopeaks belonging to RDX at 878, 1264, and 1315 cm^{-1}. The corresponding positive cross peaks are expected since the peaks are all decreasing. The negative cross peaks corresponding to the quartz and RDX autopeaks and are a consequence of the difference in behavior of the spectral features of the corresponding materials. The asynchronous plot shows a cross peak at 460 and 878 cm^{-1}, which indicates that the spectral changes of RDX and quartz are temporally separated (Figure 2.7b, right). Overlapped peaks at large Raman shift are the result of a fluorescent background that grows upon thermal treatment, similar to PETN.
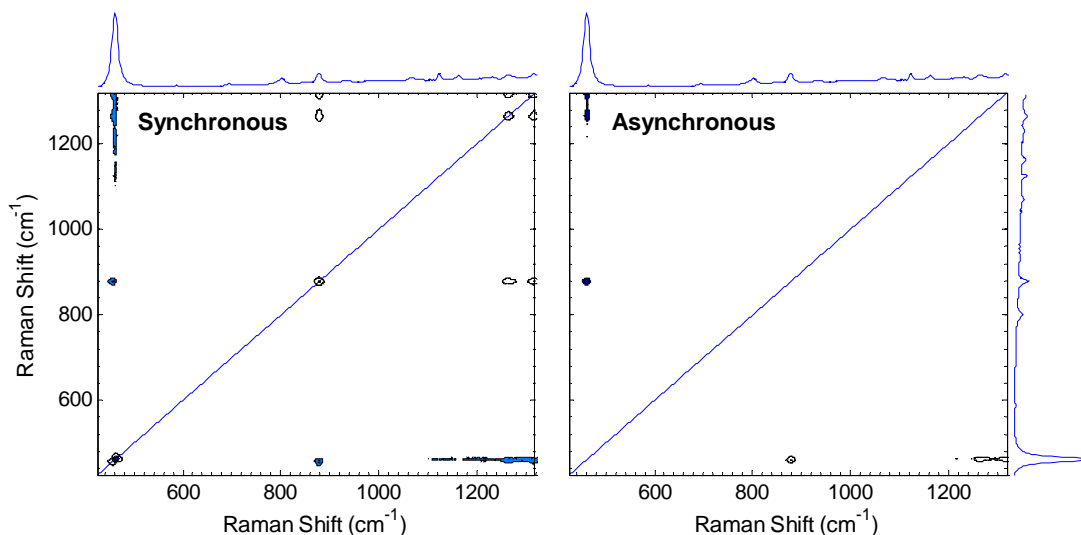
Figure 2.7 2D synchronous (left) and asynchronous (right) correlation spectra obtained from floored spectra collected during heating ramp of RDX, saliva and sand in the beam of the excitation laser. Positive and negative contours are shown as open and filled, respectively. Averaged 1D spectra are shown on the sides.

Given the likelihood of observing the non-static quartz peak in an operational environment, it would be desirable to remove it for simplification of analysis. The solitary nature of the peak makes this possible. The average of the resulting 1D spectra clearly show a number of peaks attributed to saliva (Figure 2.8a). This dataset exhibited a fluctuating, sloped background; therefore, this data is useful for re-evaluating normalization schemes in terms of maintaining the integrity of the dataset.

The results of 2D correlation analysis were compared for a dataset pretreated in two different ways: (1) only flooring and (2) flooring followed by modified mean normalization. The differences are evident in the resulting autocorrelation spectra (diagonal of 2D synchronous spectrum) in each case (Figure 2.8b and c, respectively). The three primary RDX peaks at 878, 1264, and 1315 cm^{-1}are the only features evident when no normalization is used, indicating that the saliva peaks, which do not significantly respond to thermal perturbation in this temperature range (<200 °C), are successfully filtered out

by the 2D correlation analysis. In comparison, small features at 801, 1125, and 1162 cm^{-1} that correspond to the saliva peaks become apparent with the use of modified mean- and the other normalizations examined (see Table 2.1). The nature of normalization is to assign weight to every point on a spectrum, including the peak values. When a spectrum with an increased background is normalized, intensities at all spectral variables are diminished causing an artificial depression in the peak of interest. Hence, normalization can result in artificially induced changes in otherwise static peaks and can lead to false positives.
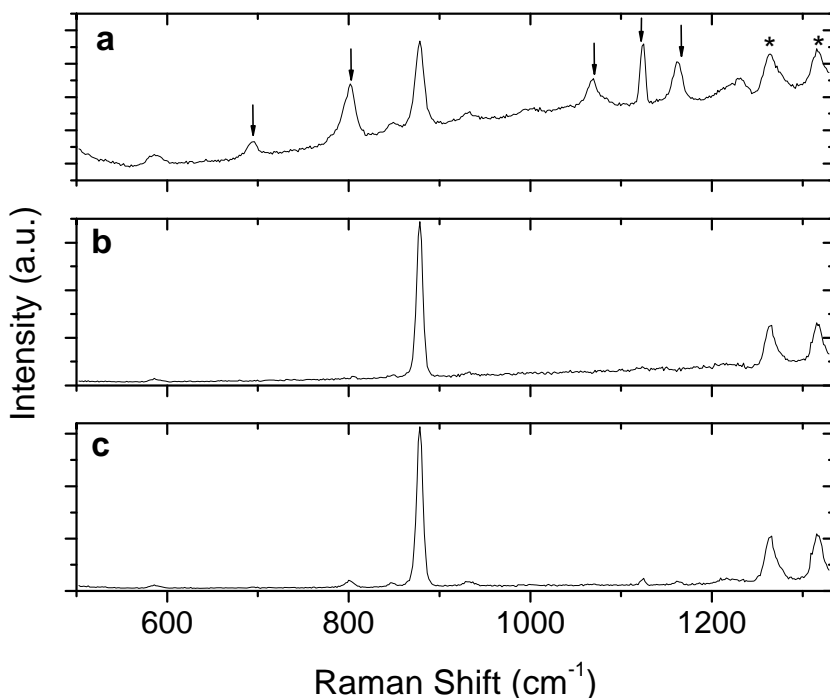
Figure 2.8 1D spectra from heating of RDX and saliva on sand: **a)** Temperature-averaged spectrum. **b)** Autocorrelation spectrum for floored spectra. **c)** Autocorrelation spectrum for floored and modified-mean-normalized spectra. Arrows indicate peaks attributed to saliva. Asterisks indicate peaks associate with nitroamine groups.

2.3.2.2 Multi-Point: RDX, Soot, Sand, Polybutadiene

The multi-point method was used in the contamination study of RDX in the presence of diesel soot, polybutadiene, and sand; all species were subjected to simultaneous

thermal treatment, while Raman spectra were collected at four different points on the sample at determined temperatures. For each temperature, the four spectra are summed and floored. The resulting 1D spectra at eight temperatures are processed using 2D correlation analysis (Figure 2.9). The spectral range was cropped to remove the quartz peak as discussed previously. The data illustrate some of the challenges anticipated in the field. For example, the primary RDX peak at 877 cm^{-1} is dwarfed by the broad feature centered at 1000 cm^{-1}, most likely due to the underlying material (here, glass slide the sample was placed on). Fortunately, the cluster of autopeaks and positive cross peaks between 1200 and 1400 cm^{-1} in the synchronous spectrum allow for the identification of RDX, as well as other nitramine compounds (Figure 2.9, left). As expected, the asynchronous spectrum shows no temporal separation between these features since they are all the result of the same chemical moiety. The sharp feature at 1122 cm^{-1} was attributed to a residue on a dirty optic. It appears to be lightly correlated with the RDX features but also with significant temporal separation. The slight wave-like behavior of scattering at high Raman shift was unchanged by heating and was the result of two broad soot bands, disorder (D) and graphitic (G), centered at approximately 1350 and 1580 cm^{-1}, respectively.[75, 76]
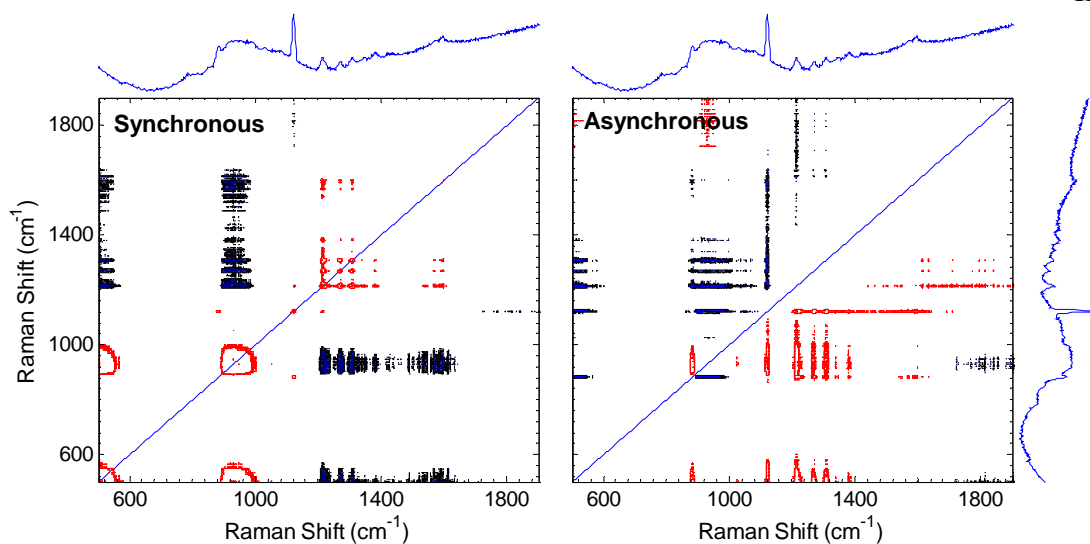
Figure 2.9 2D synchronous (left) and asynchronous (right) correlation spectra derived from the sum of spectra collected at 4 spots on a sample of trace RDX, diesel soot and PB on sand during a heating ramp. Positive and negative contours are shown as open grey and filled black, respectively. Averaged 1D spectra are shown on the sides.

2.3.2.3 Multi-Sample: PETN, Soot, Polybutadiene

In the multi-sample contamination study, individual datasets collected during separate heating of PETN, diesel soot, and bulk PB (Figure 2.10) were summed and analyzed. Although difficult to see due their large band width and low intensity, soot in this spectral range is characterized by the D and G bands at approximately 1350 and 1580 cm^{-1}.[75, 76] For PB, the majority of the spectral features in the range of interest are due to deformations of CH groups.[77] To simulate the challenges associated with detecting trace amounts of explosives in the presence of a large background, the PB contribution was scaled to be much stronger than that of PETN, as shown in Figure 2.10.
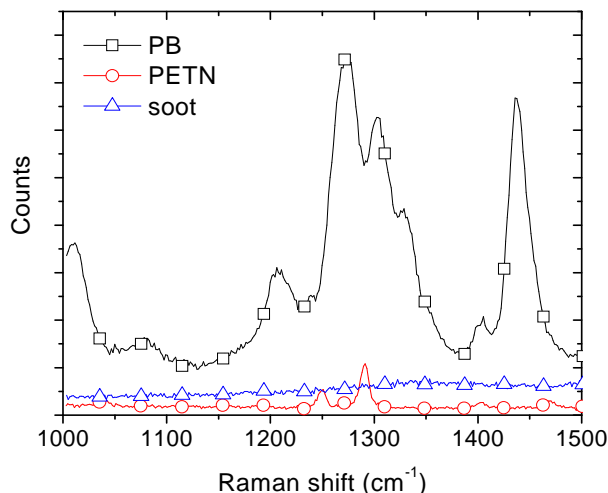
Figure 2.10 Individual spectra at room temperature of PETN, soot, and bulk PB summed to simulate identification of explosives in the presence of contaminants.

Two-dimensional plots were derived from these 1D spectra after they were summed and then floored (Figure 2.11). As expected, diesel soot was stable under the heating conditions and, as such, its features were filtered out of the 2D spectra. This was also the case if the strong PB signal was excluded (not shown). In contrast, both PB and PETN spectra exhibited changes upon heating as evidenced by the complexity of the 2D spectra (Figure 2.11). Fortunately, the disparity in stability of PB and PETN allows for their discrimination. Although the 1D spectra contain a PETN peak at 1290 cm^{-1} that is barely noticeable over the strong PB features (Figure 2.12a), the magnitude of the PETN peak in the autocorrelation spectrum is greater than surrounding features by at least a factor of three (Figure 2.12b).
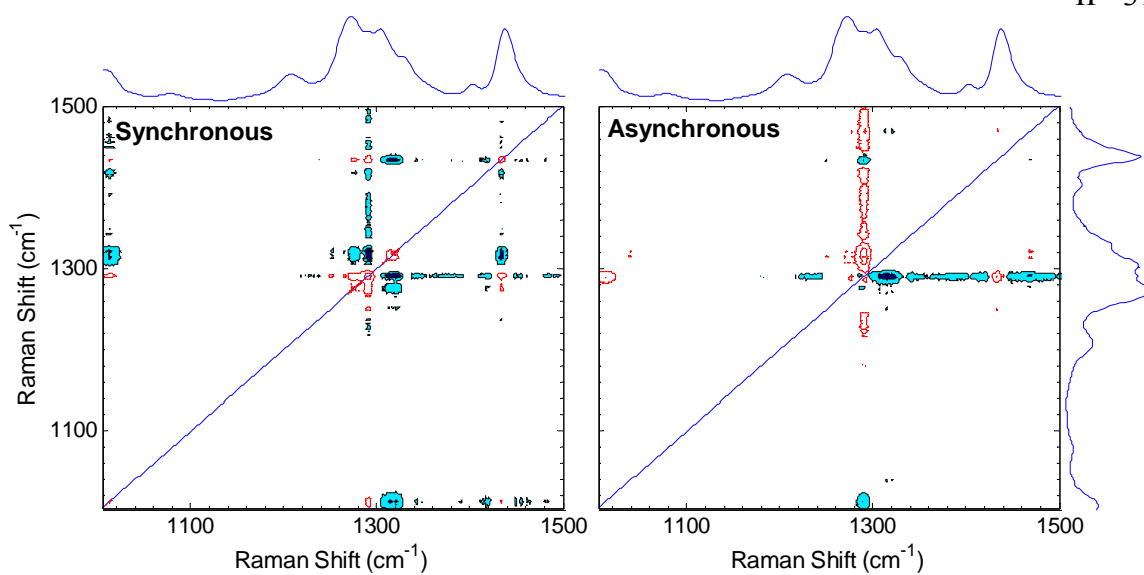
Figure 2.11 2D synchronous (left) and asynchronous (right) correlation spectra of summed and floored spectra during individual heating ramps of PETN, diesel soot, and PB. Positive and negative contours are shown open grey and filled black, respectively. Averaged 1D spectra are shown on the sides.

Autopeaks corresponding to the PB at 1275, 1329, and 1436 cm^{-1} are observed in the 2D synchronous and the autocorrelation spectra. Unlike previous results presented, positive cross peaks in the synchronous spectrum (Figure 2.11, left) are not solely due to the explosive residue. PB peaks at 1275 and 1436 cm^{-1} also appear to decrease during the heating treatment, although much less so than the PETN peak. The asynchronous spectrum shows that changes in the spectra at large Raman shift are temporally separated from the PETN features. However, as described above, these features can be attributed to the changes in fluorescence that occur during heating of neat PETN (Figure 2.5).
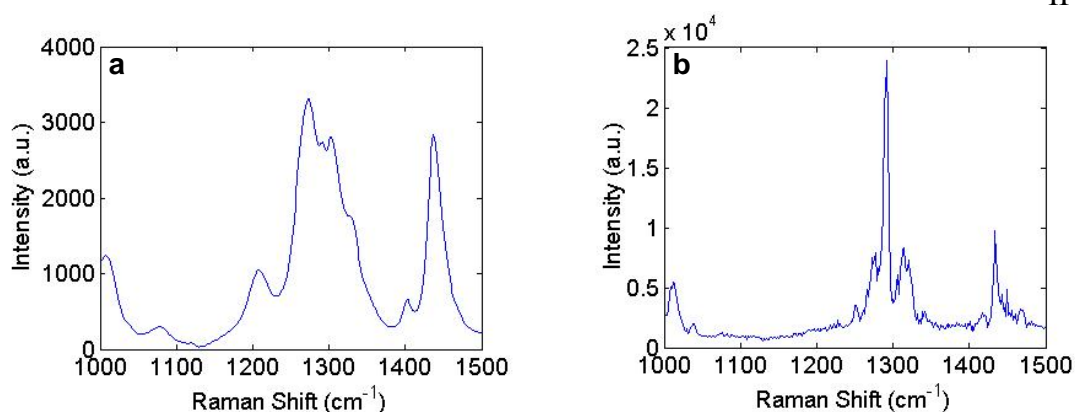
Figure 2.12 a) Average 1D spectra and **b)** autocorrelation intensity of summed and floored spectra during individual heating ramps of PETN, diesel soot, and PB.

2.3.3 Long Standoff Detection

The experiments using a conventional Raman microscope demonstrated the value of thermal decomposition in conjunction with 2D correlation analysis and highlighted the challenge posed by fluorescence. Additional enhancement in detection can be achieved by utilizing established methods to minimize fluorescence that reaches the detector. Specifically, the near instantaneous character of Raman scattering (in contrast to the relatively prolonged fluorescence emission) can be used to retain the Raman signal and reject most of the fluorescence: only the signal associated with the duration of the excitation pulse (ca. 50 ns) would be acquired. From a substantial distance, thermal modulation would be achieved optically, using successive pulses of infrared light from a CO_2 laser that is absorbed by the sand substrate. Dr. Andrew Pipino at Tanner Research. conducted experiments on RDX to test the feasibility of the long standoff system. In agreement with prior studies using a gating scheme,[13, 30, 39] spectral datasets exhibited no signs of fluorescence, which is typically a significant challenge in long standoff Raman. Additionally, the potential to induce thermal oxidation from a standoff distance was demonstrated. The intensity value at 877 cm^{-1} was used to monitor conversion of the explosive caused by

heating as a result of CO_2 laser pulses, which are strongly absorbed by the substrate (i.e., silica). In an experiment during which peak intensity dropped by 37.5%, RDX can be unambiguously identified by 2D correlation analysis of averaged spectra (Figure 2.13).
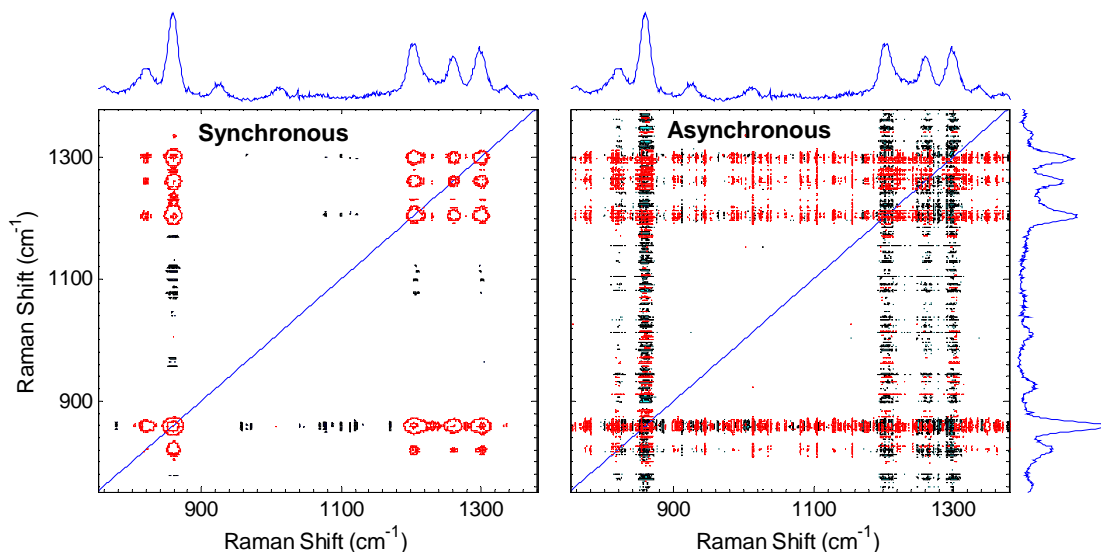
Figure 2.13 2D synchronous (left) and asynchronous (right) correlation spectra obtained without mean-normalization from long standoff measurements of RDX with a collection frequency of 1 spectrum every 10 s. Positive and negative contours are shown in open grey and filled black, respectively. Averaged 1D spectra are shown on the sides.

Due to the system averaging, which resulted in 1 spectrum every 10 seconds, direct analysis of the raw data without any pre-treatment resulted in a relatively high value of *P*. However, the individual spectra had a stationary, elevated background as the result of the amplifier used to collect the scattering signal. Flooring the dataset led to almost an order of magnitude improvement in *P* with resulting values of 690 for 2D synchronous and 65 for 1D dynamic spectra. Due to the standoff distance, the dataset contained significant random noise which is manifested in the asynchronous spectrum. Normalization by the first principal component resulted in another order of magnitude improvement in

P_{2D}. Although the noise levels were decreased by this pre-treatment, the artificial peaks in the asynchronous spectrum remained.[51]

In a separate experiment, more applicable 1-to-1 averaging (1 spectrum every 0.1 second) yielded a spectral dataset with a low average 1D dynamic P value of 2. The corresponding P_{2D} was 6. In this case, P was not affected by flooring the dataset prior to 2D correlation analysis. Normalization of the floored dataset by the first principal component resulted in a 3-fold increase in P_{2D}. Two factors led to the low P values of the 2D spectrum in this case. First, noise levels were increased due to lack of spectral averaging. Second, although there were fluctuations of intensity of the RDX peak value, a quantifiable, monotonic decrease characteristic of compound conversion was not observed during the experiment.

2.4   DISCUSSION

2.4.1 Application of 2D Correlation Analysis

The well-known susceptibility of energetic compounds to mild heating in air was demonstrated to be a valuable means to selectively perturb their spectral features, enabling 2D correlation analysis to enhance their signal in the presence of relatively static background materials. The 2D correlation spectra showed a monotonic decrease and eventual disappearance of features corresponding to explosive residues. These were relatively simple. Complications that might arise due to decomposition of explosives upon heating were not observed. This simplifying behavior can be explained by some combination of vaporization and decomposition.[78, 79] The three explosives examined (RDX, HMX, and PETN) are known to undergo vaporization below their melting points with ac-

tivation energies of 100-150 kJ/mol.[78, 80, 81] The lack of new Raman peaks can also be explained by thermal decomposition of energetic compounds that yields gas-phase products: NO, NO_2, N_2O and HCN.[82] Although trace amounts of gas could not be observed due to Raman detection limits, some material condensed on the microscope optic above the heating stage resulting in a Raman peak at 1122 cm^{-1}. Chemical reactions during heating of these compounds did produce a mild growth in fluorescence that was particularly noticeable when Raman intensities were relatively low (e.g., PETN[70]). In the case of TNT, this growth in fluorescence upon decomposition was strong enough to mask all of the expected spectral features.[83, 84] The appearance of specific reaction products when energetic compounds undergo thermal decomposition in the presence of ambient compounds cannot be excluded; however it was not observed in the presence of sand, soil, and polybutadiene (sometimes used as a plasticizer) for the military-grade explosives examined here.

The differences in the thermal stability of different energetic compounds may be used to further distinguish between them in a plastic explosive sample like C4. RDX and PETN exhibited similar responses to thermal treatment with full conversion occurring between 150 °C and 200 °C. HMX proved to be slightly less stable with decomposition/vaporization ending just above 100 °C. TNT residues were so unstable that they underwent photodecomposition at room temperature, in agreement with previous literature[14] (possibly due to the formation of electron donor-acceptor, EDA, complexes that shift the absorption maximum closer to the excitation wavelength)[85] or upon heating to only approximately 60 °C.[13] While not addressed here, the sensitivity of TNT to heating highlights the importance of selecting the proper CO_2 laser power in the long standoff system.

Heating must be sufficient to induce some vaporization/decomposition but not so much as to fully convert the energetic species with one pulse.

In the present studies, RDX, PETN, and HMX could be identified by strong autopeaks in the 2D synchronous spectra with peak intensities that were related to the magnitude of the response to the thermal modulation. Data pre-treatments can be used to enhance the discrimination of these peaks from the background. The sign of the cross peaks in the synchronous spectrum can be used to discriminate explosive peaks from features of other compounds that also responded to the thermal treatment. Although not as easily interpreted, the 2D asynchronous spectrum offers an opportunity to extract additional information for identification of peaks corresponding to energetic compounds.

2.4.1.1 Synchronous Spectra

The diagonal of the 2D synchronous spectrum contains spectral peaks that correspond to compounds that responded to the thermal modulation. The relative intensity of these autopeaks is enhanced compared to the 1D spectra and increases the probability of their detection, as demonstrated by moderate to significant improvement in the performance parameter. This is due to the nature of the 2D spectrum in which multiplication of small background values by small background values and multiplication of large peak values by large peak values results in greater separation of signal from noise. In addition to improvement in P, this separation allows the possibility of improved success of detection through the application of automated thresholding algorithms or more advanced statistical signal analysis.

In addition to strong autopeaks at the focus of calculations of the performance parameter, cross peaks are present in the synchronous spectrum between spectral features of

the same energetic compound. Unfortunately, as demonstrated by Figure 2.9 and Figure 2.11, positive cross peaks also appear for some contaminants. In this situation, examination of the corresponding asynchronous spectrum can aid in the distinction between explosive and contaminant peaks.

2.4.1.2 Asynchronous Spectra

The individual Raman signatures of a single compound undergoing vaporization/decomposition are expected to decrease and eventually disappear together. In this situation, the asynchronous spectrum should be free of peaks. Hence, it was initially surprising that asynchronous cross peaks were observed both within and between strong, 1D spectral features for all explosives examined. Both observations can be attributed to the crystalline nature of the explosive materials.

The presence of a pair of asynchronous cross peaks within one, strong 1D peak (inset of Figure 2.3) is usually due to temporal separation between overlapping bands but can also be attributed to slight peak shifting.[51] McNesby et al. reported subtle shifting of RDX Raman peaks during heating and attributed the observation to increasing lattice spacing in the crystal.[25] Hence, it is reasonable to attribute this surprising observation to the crystal nature of the compound. The existence of asynchronous peaks between strong, 1D spectral features indicates that these features are temporally separated as a result of different rates of change of those spectral features. McNesby et al. also observed uneven intensity changes between peaks of Raman spectra during heating,[25] which was attributed to the loss of crystal order at elevated temperatures.[28] Hence, the temporal separation observed for peaks of a single compound can again be attributed to the crystalline nature of the material. Since HMX and PETN are also crystalline, similar patterns are expected and

were observed in their asynchronous spectra. While details of the crystalline struc-

ture may be used to identify these materials and potentially even trace them in the future,

a profound consequence of these observations is that cross peaks evident of temporal

separation do not necessarily indicate separate species as originally anticipated.

Furthermore, interpretation of the asynchronous spectrum can be quite compli-

cated, especially in a multi-component sample. In more complex samples, the possibility

of overlapping bands and temporal separation between different species can result in

similar patterns to those described above. Hence, assignment of asynchronous peak pairs

is more ambiguous. Additionally, apparent temporal separation can be an artifact of

growing fluorescence (Figure 2.6) or improper normalization (Figure 2.8). Hence, inter-

pretation of the asynchronous spectrum must be done with care.

Nevertheless, as demonstrated in the results section, under certain conditions the

asynchronous spectrum can provide an additional level of discrimination of compounds.

These desirable conditions include (1) static background scattering, which should be at-

tainable by minimizing fluorescence with the gating employed by the long standoff sys-

tem and (2) moderate noise levels to mask the crystalline nature of the explosive materi-

als (see PETN spectra in Figure 2.6 for example). The latter condition is based on the fact

that the asynchronous peaks attributed to the crystalline nature of the material are the re-

sult of subtle changes in the Raman spectra; hence, they are very sensitive to noise. If

they are present, it may be possible to exploit this feature in order to discriminate be-

tween the two possibilities for their observation: (1) crystalline nature of compound or (2)

separate species. By inserting controlled amounts of artificial noise into the acquired 1D

spectra, asynchronous peaks resulting from the crystalline nature of a compound should be readily masked revealing more substantial changes in the spectra.

2.4.1.3 Data Pretreatments

Data pretreatments can be used to improve discrimination of signal relative to background (increase the performance parameter) and, hence, decrease the probability of overlooking a compound that is actually present (false negatives). For the current application data pretreatment should be rapid and data-blind. Standard background subtraction would require time for background collection and is not ideal for the current application. The approximation of a background would require human intervention, which is also undesirable. An alternative approach to minimize background effects is to subtract the minimum intensity value from each spectrum ('flooring'). This was effective in increasing P in most cases, except when P is already very low.

A further increase in P could be obtained through a variety of normalizations (Table 2.1). Modified mean normalization proved to be most effective for a sample displaying mild fluorescence. Ideally, fluorescence would be rejected from the acquired signal by the gating scheme. However, the challenges due to fluorescence, which are manifested as a non-stationary background (i.e., significant background contribution to 2D spectra), could be introduced by other aspects of the operating environment. While normalization minimizes background effects, artifacts are introduced to the 2D spectra (Figure 2.12).[57] Hence, cross peaks observed in synchronous and asynchronous spectra obtained from normalized data cannot be used to discriminate energetic compounds from more stable species.

Alternatively, additional enhancement of peak identification can be achieved through a pretreatment that smoothes the 1D data. The simplest smoothing algorithms should be avoided as they cannot discriminate noise from peaks when P is low. Possible algorithms might include filters based on noise perturbation in conjunction with PCA.[42] An additional requisite for the final smoothing pretreatment, as for all data manipulations for the current application, is that it require a reasonable amount of computing power.

2.4.2 Fluorescence

The presence of fluorescence affects both the quantitative (performance parameter) and qualitative (artifacts) aspects of 2D correlation spectra. Varying levels of fluorescence can be introduced by decomposition products of energetic compounds or even the products themselves.[70, 86] However, this is minor compared to the luminescence that is encountered from contaminants (e.g., urine, diesel fuel[86]) and ambient species in the operating environment.[13, 30, 71] To cope, the standoff system utilizes a gating scheme to minimize the amount of fluorescence that reaches the detector based on the disparity in lifetimes between Raman scattering (10^{-12}–10^{-13} s) and fluorescence (10^{-7}–10^{-9} s).[39, 61] Preliminary studies have demonstrated its effectiveness for a target at a fixed distance for which the delay and gate width were optimized.[13, 30, 71] However, previous studies have observed that gating is not fully effective at rejecting luminescence from some backgrounds.[30, 71] Therefore, additional attempts have been made to overcome fluorescence, which is typically 10^4 to 10^6 times greater in intensity than Raman scattering with excitation in the visible range,[87] by enhancing the Raman signal.

2.4.3 Raman Signal Enhancement

The small cross section for Raman scattering (10^{-30} to 10^{-25} cm^2/molecule)[88] has inspired attempts to enhance the signal through different techniques.[15, 27, 87, 89, 90] The simplest one, as mentioned above, is the use of a shorter excitation wavelength. Since the Raman cross section scales as the inverse of scattering wavelength to the fourth power (λ^{-4}), using a shorter wavelength will enhance the signal and decrease excitation power requirement. Additionally, the use of ultraviolet (UV) excitation energies close to those of allowed electronic transitions of the material results in resonance and pre-resonance enhancement that can overcome fluorescence.[15, 27, 71, 91] The use of deep UV excitation (<260 nm) provides the additional advantage of a fluorescence-free background since fluorescence typically occurs at longer wavelengths.[30, 87, 91]

An alternative technique to increase the Raman signal is the use of a substrate containing metallic nanostructures. Surface Enhanced Raman Spectroscopy (SERS) may be observed when particular molecules are coupled with the plasmon resonance of the metallic nanostructures of the substrate onto which they are absorbed. Research in the field of SERS is currently very active in attempts to gain full understanding of the effect so as to fully exploit it. Enhancement of signal by factors of 10^5 to 10^9 has been observed, adequate to overcome fluorescence.[92, 93] A number of attempts have been made to use SERS for detection of explosive residues.[24, 29, 94] We have conducted preliminary experiments on 25 nm gold nanoparticle arrays fabricated by Dr. David Boyd (Caltech), but no evidence of SERS was observed. Currently, there is no practical way to implement SERS for long standoff detection of explosives; however that does not rule out future applications.

2.5 CONCLUSION

Two-dimensional correlation spectroscopy in conjunction with thermal modulation was demonstrated to be an effective scheme for the detection of explosive residues via long standoff Raman Spectroscopy. Thermal modulation was found to be an effective means to perturb the Raman features of the energetic compounds. The modulated signal was enhanced through the application of 2D correlation analysis, which resulted in synchronous spectra containing autopeaks with increased explosive peak values. This increase in the 'performance parameter' can reduce both the probability of false alarm and false negatives based on automated thresholding algorithms or more advanced statistical signal analysis. In some cases, the sign of the cross peaks (positive for energetic compounds) in the synchronous spectrum can be used to further discriminate between possible energetic compounds and ambient compounds that also respond to thermal treatment. When this distinction is not effective, the asynchronous spectrum, although sometimes difficult to interpret, can provide information about temporal separation of features which can further discriminate explosive compounds.

Several data-blind pre-treatments were examined for improvement in P. Background fluctuations can be minimized to some degree by flooring data prior to 2D correlation analysis. Peak identification can be further enhanced by normalization of the 1D spectra. Improvement in P by normalizing long standoff data by the first principal component provides motivation for further testing of this technique. However, the implementation of normalization can produce artifacts when background scattering is not static, like the in the case of fluorescence. Hence, successive 1D spectra should be checked for static backgrounds if normalization is to be used.

The optimum detection range should be between 800 and 1500 cm^{-1} such that it is as small as possible for rapid detection while including key features of energetic compounds: their strongest peaks (e.g., ring stretch for RDX or HMX) as well as the distinct NO$_2$/N-N stretches of nitramine explosives. Additionally, two-dimensional correlation spectroscopy is not immune to the challenges presented by fluorescence because fluorescence is not static. Hence, the successful gating scheme implemented to collect the nearly immediate Raman scattering from relatively delayed fluorescence is imperative for the implementation of the proposed scheme.

Further studies of the effectiveness of the proposed scheme should include a range of contaminants and substrates, as well as other explosives. A number of home-made explosives are of particular interest: ammonium nitrate fuel oil (ANFO), urea nitrate (UN), triacetone triperoxide (TATP), and potassium chlorate (KCl). Some of these have the potential to be especially challenging to detect due to their similarity to common fertilizer, native fluorescence,[86] and a lack of NO$_2$ or N-N structures typical of military grade explosives.

On a final note, the strategy that is pursued—two-dimensional correlation analysis in conjunction with a thermal perturbation—may be extended to other spectroscopic techniques.

2.6   ACKNOWLEDGEMENTS

2.7 REFERENCES

1. Joint Improvised Explosive Device Defeat Organization. www.jieddo.dod.mil.

2. Moore, D. S., Instrumentation for trace detection of high explosives. *Review of Scientific Instruments* **2004,** 75, (8), 2499-2512.

3. Steinfeld, J. I.; Wormhoudt, J., Explosives detection: A challenge for physical chemistry. *Annual Review of Physical Chemistry* **1998,** 49, 203-232.

4. Bauer, C.; Sharma, A. K.; Willer, U.; Burgmeier, J.; Braunschweig, B.; Schade, W.; Blaser, S.; Hvozdara, L.; Muller, A.; Holl, G., Potentials and limits of mid-infrared laser spectroscopy for the detection of explosives. *Applied Physics B-Lasers and Optics* **2008,** 92, (3), 327-333.

5. Arusi-Parpar, T.; Heflinger, D.; Lavi, R., Photodissociation followed by laser-induced fluorescence at atmospheric pressure and 24 degrees C: a unique scheme for remote detection of explosives. *Applied Optics* **2001,** 40, (36), 6677-6681.

6. Wynn, C. M.; Palmacci, S.; Kunz, R. R.; Clow, K.; Rothschild, M. In *Detection of condensed-phase explosives via laser-induced vaporization, photodissociation, and resonant excitation*, 2008; Optical Soc Amer: 2008; pp 5767-5776.

7. Wynn, C. M.; Palmacci, S.; Kunz, R. R.; Rothschild, M., A Novel Method for Remotely Detecting Trace Explosives. *Lincoln Laboratory Journal* **2008,** 17, (2), 27-39.

8. Dikmelik, Y.; Spicer, J. B., Femtosecond laser-induced breakdown spectroscopy of explosives and explosive-related compounds. *Proceedings of the SPIE - The International Society for Optical Engineering* **2005,** 5794, (1), 757-761.

9. Hua, Z.; Redo, A.; Yunqing, C.; Xi-Cheng, Z., THz wave standoff detection of explosive materials. *Proceedings of the SPIE - The International Society for Optical Engineering* **2006,** 6212, 62120L-1-62120L-62120L-8.

10. Wentworth, R. M.; Neiss, J.; Nelson, M. P.; Treado, P. J. In *Standoff Raman hyperspectral imaging detection of explosives*, 2007 IEEE Antennas and Propagation Society International Symposium, Honolulu, HI, USA, 9-15 June, 2008; Ieee: Honolulu, HI, USA, 2008; pp 4925-4928.

11. Committee on the Review of Existing and Potential Standoff Explosives Detection Techniques, N. R. C., *Existing and Potential Standoff Explosives Detection Techniques*. The National Academies Press: Washington D.C., 2004; p 148.

12. Gottfried, J. L.; De Lucia, F. C.; Munson, C. A.; Miziolek, A. W., Strategies for residue explosives detection using laser-induced breakdown spectroscopy. *Journal of Analytical Atomic Spectrometry* **2008,** 23, (2), 205-216.

13. Carter, J. C.; Angel, S. M.; Lawrence-Snyder, M.; Scaffidi, J.; Whipple, R. E.; Reynolds, J. G., Standoff Detection of High Explosive Materials at 50 Meters in Ambient Light Conditions Using a Small Raman Instrument. *Applied Spectroscopy* **2005,** 59, (6), 769-775.

14. Carter, J. C.; Scaffidi, J.; Burnett, S.; Vasser, B.; Sharma, S. K.; Angel, S. M., Standoff Raman detection using dispersive and tunable filter based systems. *Spectrochimica Acta Part A* **2005,** 61, 2288-2298.

15. Comanescu, G.; Manka, C. K.; Grun, J.; Nikitin, S.; Zabetakis, D., Identification of explosives with two-dimensional ultraviolet resonance Raman spectroscopy. *Applied Spectroscopy* **2008,** 62, (8), 833-839.

16. Eckenrode, B. A.; Bartick, E. G.; Harvey, S. D.; Vucelick, M. E.; Wright, B. W.; Huff, R. A., Portable Raman Spectroscopy Systems for Field Analysis. *Forensic Science Communications* **2001,** 3, (4).

17. Grasso, R. J.; Russo, L. P.; Barrett, J. L.; Odhner, J. E.; Egbert, P. I., An accurate modeling, simulation, and analysis tool for predicting and estimating Raman LIDAR system performance. *Proceedings of the SPIE - The International Society for Optical Engineering* **2007,** 6681, (1), 66810D-1-66810D-66810D-18.

18. Hayward, I. P.; Kirkbride, T. E.; Batchelder, D. N.; Lacey, R. J., Use of a Fiber Optic Probe for the Detection and Identification of Explosive Materials by Raman-Spectroscopy. *Journal of Forensic Sciences* **1995,** 40, (5), 883-884.

19. Sharma, S. K.; Misra, A. K.; Sharma, B. In *Portable remote Raman system for monitoring hydrocarbon, gas hydrates and explosives in the environment*, 2005; Pergamon-Elsevier Science Ltd: 2005; pp 2404-2412.

20. Ballesteros, L. M.; Herrera, G. M.; Castro, M. E.; Briano, J.; Mina, N.; Hernandez-Rivera, S. P., Spectroscopic signatures of PETN in contact with sand particles. *Proceedings of the SPIE - The International Society for Optical Engineering* **2005,** 5794, (1), 1254-1262.

21. Fell, N. F.; Vanderhoff, J. A.; Pesce-Rodriguez, R. A.; McNesby, K. L., Characterization of Raman spectral changes in energetic materials and propellants during heating. *Journal of Raman Spectroscopy* **1998,** 29, (3), 165-172.

22. Herrera-Sandoval, G. M.; Ballesteros, L. M.; Mina, N.; Briano, J.; Castro, M. E.; Hernandez-Rivera, S. P., Raman signatures of TNT in contact with sand particles.

Proceedings of the SPIE - The International Society for Optical Engineering **2005,** 5794, (1), 1245-1253.

23. Lewis, I. R.; Daniel, N. W.; Griffiths, P. R., Interpretation of Raman spectra of nitro-containing explosive materials. Part I: Group frequency and structural class membership. *Applied Spectroscopy* **1997,** 51, (12), 1854-1867.

24. McHugh, C. J.; Keir, R.; Graham, D.; Smith, W. E., Selective functionalisation of TNT for sensitive detection by SERRS. *Chemical Communications* **2002**, (6), 580-581.

25. McNesby, K. L.; Fell, N. F., Jr.; Vanderhoff, J. A., Detection and characterization of explosives using Raman spectroscopy: identification, laser heating, and impact sensitivity. *Proceedings of the SPIE - The International Society for Optical Engineering* **1997,** 3082, 121-135.

26. Moore, D. S.; Lee, K. Y., Raman spectroscopy as a tool for long-term energetic material stability studies. *Journal of Raman Spectroscopy* **2007,** 38, (9), 1221-1224.

27. Nagli, L.; Gaft, M.; Fleger, Y.; Rosenbluh, M., Absolute Raman cross-sections of some explosives: Trend to UV. *Optical Materials* **2008,** 30, 1747-1754.

28. Reylafon, M.; Trinquec.C; Cavagnat, R.; Forel, M. T., Study on Vibration Spectra of Hexhydro-1,3,5-Trinitro Sym Triazine .1. Analysis of Infrared and Raman Spectra between 3200 and 200 Cm-1. *Journal De Chimie Physique Et De Physico-Chimie Biologique* **1971,** 68, (10), 1533-&.

29. Sylvia, J. M.; Janni, J. A.; Klein, J. D.; Spencer, K. M., Surface-enhanced Raman detection of 1,4-dinitrotoluene impurity vapor as a marker to locate landmines. *Analytical Chemistry* **2000,** 72, (23), 5834-5840.

30. Gaft, M.; Nagi, L. In *UV gated Raman spectroscopy for standoff detection of explosives*, 2008; Elsevier Science Bv: 2008; pp 1739-1746.

31. Wormhoudt, J.; Kebabian, P. L.; Kolb, C. E., Infrared fiber-optic diagnostic observations of solid propellant combustion. *Combustion and Flame* **1997,** 108, (1-2), 43-60.

32. Riris, H.; Carlisle, C. B.; McMillen, D. F.; Cooper, D. E., Explosives detection with a frequency modulation spectrometer. *Applied Optics* **1996,** 35, (24), 4694-4704.

33. Bannister, W. W.; Chen, C.-C.; Curby, W. A.; Chen, E. B.; Damour, P. L.; Morales, A. Thermal analysis for detection and identification of explosives and other controlled substances. 2004.

34. Wormhoudt, J.; Shorter, J. H.; McManus, J. B.; Kebabian, P. L.; Zahniser, M. S.; Davis, W. M.; Cespedes, E. R.; Kolb, C. E. In *Tunable infrared laser detection of pyrolysis products of explosives in soils*, 1996; Optical Soc Amer: 1996; pp 3992-3997.

35. Lemire, G. W.; Simeonsson, J. B.; Sausa, R. C., Monitoring of Vapor-Phase Nitro-Compounds Using 226-Nm Radiation - Fragmentation with Subsequent No Resonance-Enhanced Multiphoton Ionization Detection. *Analytical Chemistry* **1993,** 65, (5), 529-533.

36. Ger, M. D.; Hwu, W. H.; Huang, C. C., A Study on the Thermal-Decomposition of Mixtures Containing an Energetic Binder and a Nitramine. *Thermochimica Acta* **1993,** 224, 127-140.

37. De Lucia, F. C.; Gottfried, J. L.; Munson, C. A.; Miziolek, A. W. In *Multivariate analysis of standoff laser-induced breakdown spectroscopy spectra for classification of explosive-containing residues*, 2008; Optical Soc Amer: 2008; pp G112-G121.

38. Hua, Z.; Cunlin, Z.; Liangliang, Z.; Yuejin, Z.; Xi-Cheng, Z., A phase feature extraction technique for terahertz reflection spectroscopy. *Applied Physics Letters* **2008,** 92, (22), 221106-1-221106-221106-3.

39. Vanduyne, R. P.; Jeanmair.Dl; Shriver, D. F., Mode-Locked Laser Raman-Spectroscopy - New Technique for Rejection of Interfering Background Luminescence Signals. *Analytical Chemistry* **1974,** 46, (2), 213-222.

40. Noda, I., Generalized Two-Dimensional Correlation Method Applicable to Infrared, Raman, and Other Types of Spectroscopy. *Applied Spectroscopy* **1993,** 47, (9), 1329-1336.

41. Gericke, A.; Gadaleta, S. J.; Brauner, J. W.; Mendelsohn, R., Characterization of biological samples by two-dimensional infrared spectroscopy: Simulation of frequency, bandwidth, and intensity changes. *Biospectroscopy* **1996,** 2, (6), 341-351.

42. Hu, Y.; Li, B. Y.; Sato, H.; Noda, I.; Ozaki, Y., Noise perturbation in functional principal component analysis filtering for two-dimensional correlation spectroscopy: Its theory and application to infrared spectra of a poly(3-hydroxybutyrate) thin film. *Journal of Physical Chemistry A* **2006,** 110, (39), 11279-11290.

43. Kim, H. J.; Bin Kim, S.; Kim, J. K.; Jung, Y. M., Two-dimensional heterospectral correlation analysis of wide-angle X-ray scattering and infrared spectroscopy for specific chemical interactions in weakly interacting block copolymers. *Journal of Physical Chemistry B* **2006,** 110, (46), 23123-23129.

44. McNavage, W.; Dai, H. L., Two-dimensional cross-spectral correlation analysis and its application to time-resolved Fourier transform emission spectra of transient radicals. *Journal of Chemical Physics* **2005,** 123, (18), 12.

45. Meng, S.; Sun, B.; Guo, Z.; Zhong, W.; Du, Q.; Wu, P., Two-dimensional cor-relation ATR-FTIR studies on PEO–PPO–PEO tri-block copolymer and its phos-phorylcholine derivate as thermal sensitive hydrogel systems. *Polymer* **2008,** 49, 2738-2744.

46. Murayama, K.; Czarnik-Matusewicz, B.; Wu, Y.; Tsenkova, R.; Ozaki, Y., Compari-son between Conventional Spectral Analysis Methods, Chemometrics, and Two-Dimensional Correlation Spectroscopy in the Analysis of Near-Infrared Spectra of Protein. *Applied Spectroscopy* **2000,** 54, (7), 978-985.

47. Nabet, A.; Auger, M.; Pezolet, M., Investigation of the temperature behavior of the bands due to the methylene stretching vibrations of phospholipid acyl chains by two-dimensional infrared correlation spectroscopy. *Applied Spectroscopy* **2000,** 54, (7), 948-955.

48. Noda, I. In *Recent advancement in the field of two-dimensional correlation spectros-copy*, 2008; Elsevier Science Bv: 2008; pp 2-26.

49. Noda, I.; Allen, W. M.; Lindberg, S. E., Two-Dimensional Raman Correlation Spec-troscopy Study of an Emulsion Copolymerization Reaction Process. *Applied Spec-troscopy* **2009,** 63, (2), 224-232.

50. Noda, I.; Ozaki, Y., *Two-Dimensional Correlation Spectroscopy*. John Wiley & Sons Ltd.: West Sussex 2004.

51. Czarnecki, M. A., Interpretation of two-dimensional correlation spectra: Science or art? *Applied Spectroscopy* **1998,** 52, (12), 1583-1590.

52. Hu, Y.; Zhang, Y.; Li, B. Y.; Ozaki, Y., Application of sample-sample two-dimensional correlation spectroscopy to determine the glass transition temperature of poly(ethylene terephthalate) thin films. *Applied Spectroscopy* **2007,** 61, (1), 60-67.

53. Yu, Z. W.; Noda, I., On the normalization method in two-dimensional correlation spectra when concentration is used as a perturbation parameter. *Applied Spectroscopy* **2003,** 57, (2), 164-167.

54. Czarnecki, M. A., Two-dimensional correlation spectroscopy: Effect of normalization of the dynamic spectra. *Applied Spectroscopy* **1999,** 53, (11), 1392-1397.

55. Noda, I.; Ozaki, Y., Response to "some comments on tine application of two-dimensional correlation spectroscopy and normalization of the dynamic spectra" by Miroslaw A. Czarnecki. *Applied Spectroscopy* **2003,** 57, (1), 110-112.

56. Czarnecki, M. A., Some comments on the application of two-dimensional correlation spectroscopy and normalization of the dynamic spectra. *Applied Spectroscopy* **2003,** 57, (1), 107-109.

57. Diewok, J.; Ayora-Canada, M. J.; Lendl, B., 2D correlation spectroscopy and multivariate curve resolution in analyzing pH-dependent evolving systems monitored by FT-IR spectroscopy, a comparative study. *Analytical Chemistry* **2002,** 74, (19), 4944-4954.

58. Czarnecki, M. A., Two-dimensional correlation spectroscopy: Effect of reference spectrum on noise-free and noisy spectra. *Applied Spectroscopy* **2003,** 57, (8), 991-995.

59. Sasic, S.; Muszynski, A.; Ozaki, Y., A new possibility of the generalized two-dimensional correlation spectroscopy. 1. Sample-sample correlation spectroscopy. *Journal of Physical Chemistry A* **2000,** 104, (27), 6380-6387.

60. Shinzawa, H.; Morita, S.; Noda, I.; Ozaki, Y. In *Effect of the window size in moving-window two-dimensional correlation analysis*, 2006; Elsevier Science Bv: 2006; pp 28-33.

61. Ferraro, J. R.; Nakamoto, K.; Brown, C. W., *Introductory Raman Spectroscopy*. second ed.; Academic Press: Boston, 2003.

62. Noda, I., Determination of Two-Dimensional Correlation Spectra Using the Hilbert Transform. *Applied Spectroscopy* **2000,** 54, (7), 994-999.

63. Sasic, S.; Ozaki, Y., Comparison of principal component analysis and generalized two-dimensional correlation spectroscopy: Spectral analysis of synthetic model system and near-infrared spectra of milk. *Applied Spectroscopy* **2001,** 55, (1), 29-38.

64. Wang, Y. W.; Gao, W. Y.; Noda, I.; Yu, Z. W. In *A modified mean normalization method to reduce the effect of peak overlap in two-dimensional correlation spectroscopy*, 2006; Elsevier Science Bv: 2006; pp 128-133.

65. Wang, Y. W.; Gao, W. Y.; Wang, X. G.; Yu, Z. W. In *A novel normalization method based on principal component analysis to reduce the effect of peak overlaps in two-dimensional correlation spectroscopy*, 2008; Elsevier Science Bv: 2008; pp 66-72.

66. Goormaghtigh, E.; Ruysschaert, J. M.; Raussens, V., Evaluation of the information content in infrared spectra for protein secondary structure determination. *Biophysical Journal* **2006,** 90, (8), 2946-2957.

67. Frank, J., *Three-Dimensional Electron Microscopy of Macromolecular Assemblies*. 2 ed.; Oxford University Press: Oxford, 2006.

68. Shlens, J. *A Tutorial on Principal Component Analysis*; 2005.

69. Iqbal, Z.; Bulusu, S.; Autera, J. R., Vibrational-Spectra of Beta-Cyclotetramethylene Tetranitramine and Some of Its Isotopic Isomers. *Journal of Chemical Physics* **1974,** 60, (1), 221-230.

70. Aduev, B. P.; Belokurov, G. M.; Grechin, S. S.; Tupitsin, E. V., Electron beam induced explosive luminescence of PETN. *Technical Physics Letters* **2004,** 30, (8), 660-662.

71. Nagli, L.; Gaft, M., Raman scattering spectroscopy for explosives identification. *Proceedings of the SPIE - The International Society for Optical Engineering* **2007,** 6552, (1), 65520Z-1-65520Z-65520Z-10.

72. Cherney, D. P.; Ekman, D. R.; Dix, D. J.; Collette, T. W., Raman Spectroscopy-Based Metabolomics for Differentiating Exposures to Triazole Fungicides Using Rat Urine. In 2007; Vol. 79, pp 7324-7332.

73. Ichikawa, S.; Suda, J.; Sato, T.; Suzuki, Y., Lattice dynamics and temperature dependence of the first-order Raman spectra for alpha-SiO2 crystals. *Journal of Raman Spectroscopy* **2003,** 34, (2), 135-141.

74. Shapiro, S. M.; Oshea, D. C.; Cummins, H. Z., Raman Scattering Study of Alpha-Beta Phase Transition in Quartz. *Physical Review Letters* **1967,** 19, (7), 361-&.

75. Knauer, M.; Carrara, M.; Rothe, D.; Niessner, R.; Ivleva, N. P., Changes in Structure and Reactivity of Soot during Oxidation and Gasification by Oxygen, Studied by Mi-

cro-Raman Spectroscopy and Temperature Programmed Oxidation. *Aerosol Science and Technology* **2009,** 43, (1), 1-8.

76. Brunetto, R.; Pino, T.; Dartois, E.; Cao, A. T.; d'Hendecourt, L.; Strazzulla, G.; Brechignac, P., Comparison of the Raman spectra of ion irradiated soot and collected extraterrestrial carbon. *Icarus* **2009,** 200, (1), 323-337.

77. Cornell, S. W.; Koenig, J. L., Raman Spectra of Polybutadiene Rubbers. *Macromolecules* **1969,** 2, (5), 540-&.

78. Long, G. T.; Vyazovkin, S.; Brems, B. A.; Wight, C. A., Competitive vaporization and decomposition of liquid RDX. *Journal of Physical Chemistry B* **2000,** 104, (11), 2570-2574.

79. Ng, W. L.; Field, J. E.; Hauser, H. M., Thermal, Fracture, and Laser-Induced Decomposition of Pentaerythritol Tetranitrate. *Journal of Applied Physics* **1986,** 59, (12), 3945-3952.

80. Zenin, A. A.; Finjakov, S. V., Characteristics of RDX combustion zones at different pressures and initial temperatures. *Combustion Explosion and Shock Waves* **2006,** 42, (5), 521-533.

81. Pitchimani, R.; Zheng, W.; Simon, S. L.; Hope-Weeks, L. J.; Burnham, A. K.; Weeks, B. L. In *Thermodynamic analysis of pure and impurity doped pentaerythritol tetranitrate crystals grown at room temperature*, 2007; Springer: 2007; pp 475-478.

82. Adams, G. F.; Shaw, R. W., Chemical-Reactions in Energetic Materials. *Annual Review of Physical Chemistry* **1992,** 43, 311-340.

83. Oxley, J. C.; Smith, J. L.; Zhou, Z. L.; McKenney, R. L., Thermal-Decomposition Studies on Nto and Nto/Tnt. *Journal of Physical Chemistry* **1995,** 99, (25), 10383-10391.

84. Tanaka, J.; Yoshihara, K., Absorption and Fluorescence Spectra of Anthracene-s-Trinitrobenzene Complex Crystal. *Bulletin of the Chemical Society of Janpan* **1965,** 38, (5), 739-745.

85. Sharma, S. P.; Lahiri, S. C., Absorption spectroscopic and FTIR studies on EDA complexes between TNT (2,4,6-trinitrotoluene) with amines in DMSO and determination of the vertical electron affinity of TNT. *Spectrochimica Acta Part a-Molecular and Biomolecular Spectroscopy* **2008,** 70, (1), 144-153.

86. Phifer, C. C.; Schmitt, R. L.; Thorne, L. R.; Jr., P. H.; Parmeter, J. E. *Studies of the Laser-Induced Fluorescence of Explosives and Explosive Compositions*; Sandia National Laboratories: October 2006, 2006.

87. Hug, W. F.; Bhartia, R.; Tsapin, A.; Lane, A.; Conrad, P.; Sijapati, K.; Reid, R. D., Water and surface contamination monitoring using deep UV laser induced native fluorescence and Raman spectroscopy. *Proceedings of the SPIE - The International Society for Optical Engineering* **2006,** 6378, (1), 63780S-1-63780S-63780S-13.

88. Kneipp, K.; Kneipp, H.; Itzkan, I.; Dasari, R. R.; Feld, M. S., Ultrasensitive chemical analysis by Raman spectroscopy. *Chemical Reviews* **1999,** 99, (10), 2957-+.

89. Lal, S.; Grady, N. K.; Kundu, J.; Levin, C. S.; Lassiter, J. B.; Halas, N. J., Tailoring plasmonic substrates for surface enhanced spectroscopies. *Chemical Society Reviews* **2008,** 37, 898-911.

90. Le, F.; Brandl, D. W.; Urzhumov, Y. A.; Wang, H.; Kundu, J.; Halas, N. J.; Aizpurua, J.; Nordlander, P., Metallic Nanoparticle Arrays: A Common Substrate for Both Surface-Enhanced Raman Scattering and Surface-Enhanced Infrared Absorption. *ACS Nano* **2008,** 2, (4), 707-718.

91. Asher, S. A.; Johnson, C. R., Raman-Spectroscopy of a Coal Liquid Shows That Fluorescence Interference Is Minimized with Ultraviolet Excitation. *Science* **1984,** 225, (4659), 311-313.

92. Moskovits, M., Surface-Enhanced Spectroscopy. *Reviews of Modern Physics* **1985,** 57, (3), 783-826.

93. Polavarapu, L.; Xu, Q.-H., Water-Soluble Conjugated Polymer-Induced Self-Assembly of Gold Nanoparticles and Its Application to SERS. *Langmuir* **2008,** 24, 10608-10611.

94. Kneipp, K.; Wang, Y.; Dasari, R. R.; Feld, M. S.; Gilbert, B. D.; Janni, J.; Steinfeld, J. I., Near-infrared surface-enhanced Raman scattering of trinitrotoluene on colloidal gold and silver. *Spectrochimica Acta Part a-Molecular and Biomolecular Spectroscopy* **1995,** 51, (12), 2171-2175.